# Sulfur-containing particles emitted by concealed sulfide ore deposits: An unknown source of sulfur-containing particles in the atmosphere

Jianjin Cao[a,b]*, Yingkui Li[a], Tao Jiang[a], Guai Hu[a]

a School of Earth Science and Geological Engineering, Sun Yat-sen University, Guangzhou, People's Republic of China 510275

b Guangdong Key Laboratory of Geological Process and Mineral Resources Exploration, Guangzhou, Guangdong 510275, P.R. China

## Abstract

Sources of sulfur dioxide, sulfates, and organic sulfur compounds, such as fossil fuels, volcanic eruptions, and animal feeding operations, have attracted considerable attention. In this study, we collected particles carried by geogas flows ascending through soil, geogas flows above the soil that had passed through the soil, and geogas flows ascending through deep faults of concealed sulfide ore deposits and analyzed them using transmission electron microscopy. Numerous crystalline and amorphous sulfur-containing particles or particle aggregations were found in the ascending geogas flows. In addition to S, the particles contained O, Ca, K, Mg, Fe, Na, Pb, Hg, Cu, Zn, As, Ti, Sr, Ba, Si, etc. Such particles are usually a few to several hundred nanometers in diameter with either regular or irregular morphology. The sulfur-containing particles originated from deep-seated weathering or faulting products of concealed sulfide ore deposits. The particles suspended in the ascending

geogas flow migrated through faults from deep-seated sources to the atmosphere. This is a previously unknown source of the atmospheric particles. This paper reports, for the first time, the emission of sulfur-containing particles into the atmosphere from concealed sulfide ore deposits. The climatic and ecological influences of these sulfur-containing particles and particle aggregations should be assessed.

Keywords: sulfur-containing particles, ascending gas flow, unknown source, sulfide ore deposits.

*Corresponding author. Tel.: 862084035033; Fax: 862084035033

E-mail address: eescjj@mail.sysu.edu.cn

## 1. Introduction

Sources of sulfur oxides, sulfates, and organic sulfur compounds are diverse and associated with natural and anthropogenic activities. Known sources of sulfur are volatile sulfur compounds derived from animal feeding operations (Trabue et al., 2008), and aerobic decomposition of food waste (Wu et al., 2010), biogenic sulfur from rice paddies (Yang et al., 1996; Yang et al., 1998) and the Subantarctic and Antarctic Oceans (Berresheim, 1987), sulfur gas ($H_2S$ and $SO_2$) from geothermal fields (Kristmannsdottir et al., 2000), organic sulfur compounds from sediments and immature crude oil (Sinninghe Damsté et al., 1988), sulfur oxides from the oxidation of fossil fuels (Soleimani et al., 2007), and sulfur dioxide from acid factories and volcanic eruptions (Wong 1978; Sweeney et al., 2008). Sulfate particles, which are important anthropogenic aerosols and influencing climate (Pósfai et al., 1997; Williams et al., 2001). Furthermore, volcanic activity is a major contributor of sulfur to the atmosphere (Zreda-Gostynska et al., 1993; Graf et al., 1998; Streets et al., 2000; Seino et al., 2004; Bhugwant et al., 2009; Bao et al., 2010; Gierén and Querol, 2010), particularly in countries such as Japan, Indonesia, Réunion Island, the Philippines, Iceland, Guatemala, and New Zealand (Rose et al., 1986; Andres et al., 1993; Streets et al., 2000; Seino et al., 2004; Chenet et al., 2005; Bhugwant et al., 2009).

Stratospheric sulfur adds very little to the environmental consequences of the anthropogenic sulfur that is released in the troposphere and deposits within days to weeks (Wong, 1978; Chenet et al., 2005). Existing research shows that $SO_2$ is oxidized to $SO_4^{2-}$ in both the gas and liquid phases. Moreover, sulfate aerosols can

55 directly affect the climate (Graf et al., 1998). In our previous work, particles carried
56 by an ascending geogas flow in the soil (Holub et al., 1999, 2001; Cao et al., 2009,
57 2010b; Cao et al., 2011; Liu et al., 2011; Wei et al., 2013) were studied and found to
58 contain sulfur. Further research showed that sulfur-containing particles carried by
59 ascending geogas flows can be transported through the soil layers and into the
60 atmosphere. Sulfur-containing particles suspended in the ascending geogas flow
61 migrate through faults from deep-seated concealed sulfide ore deposits to the Earth's
62 surface. These particles are a previously unknown source of sulfur-containing
63 particles in the atmosphere. This paper reports, for the first time, the emission of
64 sulfur-containing particles into the atmosphere from concealed sulfide ore deposits.
65 Because concealed sulfide ore deposits are widely distributed, the influence of
66 sulfur-containing particles derived from them is important. The climatic and
67 ecological effects of these particles should be studied.

68 2. Methods

69 Particles carried by an ascending geogas flow above the soil (that had flown through
70 the soil), in the soil, and in deep-seated faults were collected at the Dongshengmiao
71 polymetallic sulfide deposit in the Inner Mongolia Autonomous Region, China.
72 Particles carried by the ascending gas flow in the soil were also collected at other
73 concealed ore deposits containing sulfide minerals, such as the Kafang copper deposit
74 of the southern Yunnan Province, the Yongshengde copper deposit in northeastern
75 Yunnan, and the Qingmingshan copper–nickel sulfide deposit in Guangxi Province,
76 China.

77 Particles transported by the ascending geogas flow above the soil (that had flown
78 through the soil) were sampled using stainless steel tubes and carbon-coated nickel
79 transmission electron microscopy (TEM) grids. The length of the stainless steel tubes
80 was 40 cm and their diameter was 2.8 cm. These tubes were inserted vertically into
81 the soil to a depth of about 30 cm. A carbon-coated nickel TEM grid was fixed at the
82 end of the stainless steel tubes. The ascending geogas flow in the soil moved into the
83 stainless steel tubes and naturally passed through the 30 cm soil layer. Then, the gas
84 flow passed through the 10 cm of the empty stainless steel tubes above the soil.
85 Finally, the geogas flow arrived at the top of the tubes. Particles carried by the geogas
86 flow were adsorbed onto the carbon-coated nickel TEM grid. A protective device was
87 installed on the outside of the steel tubes to ensure that particles sampled were those
88 carried by the ascending geogas flow. The protective device is a cylindrical
89 polyethyleneterephthalate bottle. A small hole at the side of the bottle allowed the
90 outflow of ascending geogas flow; however, adsorption material placed in the hole did
91 not allow the external particles to enter. Sampling devices were installed between July
92 25, and August 23, 2013, and the carbon-coated nickel TEM grids were retrieved on
93 September 8, 2013. Sampling sites were distributed across a fault above the concealed
94 sulfide ore bodies of the Dongshengmiao polymetallic sulfide deposit.
95 Particles transported by the ascending geogas flow in the soil were collected using
96 ordinary plastic funnels. An inverted funnel was inserted in a hole that was 60–80 cm
97 deep and backfilled with soil, and a TEM grid was fixed at the end of the funnel spout
98 with nylon net. The setup was protected from contamination using plastic pipes and

cups. The TEM grids were retrieved after 60 days.

Particles carried by ascending geogas flows in deep-seated faults were sampled using two methods. The first method used an active sampling device with a vacuum pump, polyvinyl chloride (PVC) pipe and carbon-coated nickel TEM grid as the main components. One end of the PVC pipe was connected with a tubing to the pump. A drilling steel was inserted slantwise into the fault. The inserted depth was 30–50 cm. As the drilling steel was pulled out, the PVC pipe was inserted into the hole. The PVC pipe was compacted using fault gouge. The impurity gases in the PVC pipe were pumped out using the vacuum pump, then, the PVC pipe was quickly sealed. A day later, we connected a tube equipped with a carbon-coated nickel TEM grid to the PVC pipe. The gas was pumped using a vacuum pump and flowed through the TEM grid for 1 to 2 hours. Particles carried by the gas were collected by the TEM grid. Finally, the carbon-coated nickel TEM grid was removed and sealed in a sample cell. The second method did not use a vacuum pump. A carbon-coated nickel TEM grid was fixed to the end of the PVC pipe. The ascending geogas flow in the fault flowed into the PVC pipe and arrived at the top of the PVC pipe naturally. The particles carried by the geogas flows in the faults were adsorbed onto the carbon-coated nickel grid. The sampling devices were installed on August 3–10, 2013, and the TEM grids were retrieved on September 7, 2013.

High-resolution TEM analyses were performed using a Tecnai G2 F30 S-TWIN instrument at Yangzhou University, China, using an accelerating voltage of 300 kV. The grids were checked using TEM before sampling to ensure they were devoid of

particles.

## 3. Results

### 3.1 Sulfur-containing particles carried by an ascending geogas flow above the soil (that had flown through the soil)

According to the TEM analysis, particles containing high levels of S, O, Pb, Zn, Fe, Hg, As, etc, were found in the ascending gas flows above the soil above the Dongshengmiao polymetallic sulfide deposit. Table 1 provides the number of sulfur-containing particles or particle aggregations that were found on the 100 μm × 100 μm TEM grid. In general, one aggregation included more than five particles. Figure 1 shows an elliptical particle (ID: 1) having a diameter of 500 nm. The particle contains 78.17% S and 18.47% O (Table 2). Its O to S atomic ratio is 0.47. Figure 2 shows a particle aggregation (ID: 2) that consists of several small particles having a diameter of 3–8 nm. It contains 31.23% S and 59.29% Hg. The spacing of the lattice fringes was measured to be 0.333 nm. Figure 3 shows particle aggregations (ID: 3) with sizes of less than 100 nm. Their O to S atomic ratio is 0.51. The particle aggregations contain 14.48% Pb. The particle (ID: 4) illustrated in Figure 4 is elliptical with a diameter of 200 nm and contains 18.55% As, 54.2% Pb, and 8.34% Zn. The particle (ID: 5) shown in Figure 5 contains 2.25% Co. It is amorphous and has an O to S atomic ratio of 2.91. The particle aggregation (ID: 6) illustrated in Figure 6 contains 62.39% Cu and consists of small particles each having a diameter of 5–10 nm. Figure 7 presents a particle aggregation (ID: 7) that consists of many small particles with diameters of about 5 nm, and contains 69.28% Pb.

143 3.2 Sulfur-containing particles carried by an ascending gas flow in the soil

144 Numerous sulfur-containing particles transported by an ascending gas flow were
145 found in the soil over sulfide ore deposits. Figure 8 shows an aggregation of such
146 particles from the Dongshengmiao polymetallic sulfide deposit. The aggregation (ID:
147 8) may be composed of $CaSO_4$ with trace amounts of K, Mg, Fe, and Si. It is regularly
148 shaped and 300 nm in size. The selected area electron diffraction pattern shows that
149 the aggregation is polycrystalline, possibly gypsum. Figure 9 shows a TEM image of
150 a sulfur-containing particle (ID: 9) from the Kafang copper deposit, South China.
151 Sulfur accounts for 63.99% of the particle (Table 3), and its O to S atomic ratio is 0.83.
152 Its K content is 8.93%, and its size is 330 nm. Figure 10 shows a regularly polygonal
153 particle (ID: 10) from the Yongshengde copper deposit, China. Its O to S atomic ratio
154 is 3.60, and its Fe and F contents are 9.94% and 1.71%, respectively. Figure 11 shows
155 a sulfur-containing particle (ID: 11) from the Qingmingshan Cu–Ni sulfide deposit,
156 Guangxi Province, China. Its O to S atomic ratio is 2.51. The particle contains 2.03%
157 Co and is 300 nm × 400 nm in size. The selected area electron diffraction pattern
158 shows that the particle is amorphous.

159 3.3 Sulfur-containing particles carried by ascending geogas flows in deep-seated
160 faults

161 Sulfur-containing particles were found in samples obtained using two methods from
162 the deep fault gas of the Dongshengmiao polymetallic sulfide deposit. Figure 12
163 shows a sulfur-containing particle aggregation (ID: 12) that was obtained using the
164 vacuum pump from the deep-seated fault gas near a concealed ore body. The

aggregation contains O, Na, Si, S, K, Fe, Zn, and Pb. The S content is 23.8%. Figure 13 shows a particle aggregation (ID: 13) that was obtaied using a PVC pipe from a fault near a concealed ore body. The ascending gas flow arrived at the top of the PVC pipe naturally, and the particles were adsorbed by a TEM nickel grid. The particle aggregation consists of many small particles that are 4–15 nm in diameter. The small particles are elliptical and crystalline, with 0.302 nm spacing of the lattice fringes, and and their main components are O and S. Figure 14 shows a sulfur-containing particle (ID: 14) that was sampled using a PVC pipe in a fault above a concealed ore body. The vertical distance from the sample to the concealed ore body was 85 m. The vertical distance from the sample to the Earth's surface was 230 m.

3.4 Sulfur-containing particles in deep-seated fault gouges and oxidized ores

Sulfur-containing particles were also found in deep-seated fault gouges and oxidized zones of the Dongshengmiao polymetallic sulfide deposit. For example, Figure 15 shows a sulfur-containing particle (ID: 15) from the oxidized zone. According to its atomic percentage, it contains $SO_4^{2-}$ and may be Sr, Ba sulfate, and Ti oxide. Its size is 200 nm × 400 nm. Figure 16 shows a rhombus-shaped particle (ID: 16) from a deep-seated fault gouge. Its main components are O, S, and Ca, with minor amounts of Fe, Co, and Si.

Overall, the sulfur-containing particles or particle aggregations transported by ascending geogas flows can be both regular and irregular in shape and either crystalline or amorphous. The particles or particle aggregations contain Ca, K, Mg, Fe, Na, Pb, Hg, Cu, Zn, As, Ti, Sr, Ba, and Si, as well as O and S.

The number of sulfur-containing particles in the ascending geogas flows in non-sulfur-rich areas is much lower than that from the sulfide ore deposits. Furthermore, the overwhelming majority of particles in non-sulfur-rich areas have a low sulphur content. These areas are different from those with the sulfide ore deposits, in which sulfur-containing particles are densely distributed and are present at high levels in the ascending geogas flows.

## 4. Discussion and conclusions

Gold particles are formed by post-mineralization fault activity, oxidation, and bacterial weathering of primary minerals (Cao et al., 2010a). Deep-seated gold particles can be transported to the surface by an ascending gas flow, as Brownian motion enables the gold particles in the ascending gas flow to overcome the effect of gravity (Cao et al., 2010a; Cao, 2011). We assume that the same mechanism applies to sulfur-containing particles or particle aggregations. Primary sulfur-containing minerals are transformed into particles by epigenetic reworking, such as post-mineralization fault activity, in which $S^{2-}$ in the sulfide minerals is oxidized to $S^{6+}$. In this study, the sulfur-containing particles from fault gouges and oxidized ores were found, indicating that these particles were formed by the faulting and oxidation of ores. Faulting and oxidation are well-developed in the Dongshengmiao polymetallic sulfide deposit and other sulfide deposits. This finding indicates that faulting and oxidation play an important role in particle formation.

Sulfur-containing particles may be transported to the surface by an ascending geogas flow through faults (Etiope and Martinelli, 2002; Cao et al., 2010a). Material carried

by an ascending geogas flow in the soil in the Xuanhan gas field, Sichuan Province, China was sampled and measured using an instrumental neutron activation analysis. Analysis of trace element anomalies has shown the gas-bearing ring fracture structure to be 4000 m deep, suggesting that particles carried by an ascending geogas flow can be transported over long distances (Yang et al., 2000). The gas flow migrates upward because of the temperature difference and the pressure differences between the Earth's interior and its surface is the reason that the gas flow migrate upward (Tong and Li, 1999; Etiope and Martinelli, 2002; Cao et al., 2010a). In this study, Sulfide-containing particles suspended in gas above the soil were found, showing that these particles can move through the soil and get into the atmosphere.

The probability that these particles are transported by an ascending geogas flow originating in the soil is low. In the study area, the soil consists of kaolinite, halloysite, montmorillonite, illite, chlorite, hematite, quartz, goethite, and similar minerals. Kaolinite is the main mineral, and the sulfur content in the soil is low. Therefore, this soil is clearly not a probable source of sulfur-containing particles transported by an ascending geogas flow. Furthermore, there is no correlation between the numbers of these particles and those of sulfur-containing particles in the soil solid phase. Sulfur-containing particles are clearly enriched in soils above deep sulfur-rich sources because sulfur-containing particles transported by an ascending geogas flow were found in 16 deep sulfide ore bodies that were studied. This result indicates a close relationship between sulfur-containing particles in the gas flow and deep-seated sulfide ore bodies. Other rock types, such as limestone, siltstone, sandstone, and

mudstone, do not contain sufficient sulfur to become sources of sulfur-containing particles in an ascending gas flow; for example, the mean sulfur concentrations of the Devonian limestone, mudstone, siltstome, and sandstone in the northern Guangdong Province, China are $610 \times 10^{-6}$ (68 samples), $80 \times 10^{-6}$ (25 samples), $160 \times 10^{-6}$ (33 samples), and $110 \times 10^{-6}$ sulfur (4 samples), respectively.

The estimated rate of degassing for the Dongshengmiao deposit calculated to be 2.325 $m^3 s^{-1}$.The mean sulfur content of the particles carried by the ascending geogas flow for the Dongshengmiao deposit was calculated according to 45 $mg/m^3$ (Supplement). The estimated annual sulfur emission from particles in the deposit was 3.254 tons. Qi et al. (2007) reported a flue gas amount of 527300 $m^3 h^{-1}$ from the Huhehaote power plant in China and an exit particle concentration of 43.3 mg $m^{-3}$ carried by the flue gas. The $SO_3$ distribution range in fly ash in 14 power plants (e.g.,Tangshan power plant, Gaojing power plant, and Zhengzhou power plant) was reported to range between 0 and 1.05 %. The mean $SO_3$ and sulfur contents in fly ash were 0.27 % and 0.108 %, respectively. On the basis of these mean values, 21.305 tons of annual particulate sulfur emission occurred from the flue gas in the Huhehaote power plant. The annual sulfur emission from the particles carried by ascending geogas flow in the Dongshengmiao deposit was less than carried by the flue gas in the Huhehaote power plant. However, the amount of concealed deposits is much more than that of coal-burning power plants. Moreover, size of the particles carried by the ascending geogas flow from concealed deposits is usually <500 nm. The mean diameter of the particles carried by the flue gas in 9 samples obtained from four coal-fired power

plants in China were 19.71, 3.18, 5.43, 5.67, 130.94, 77.29, 12.99, 11.59, and 236.63 μm respectively (Zhang et al. 2007). The sizes of particles carried by the ascending geogas flow from concealed deposits were lesser than those of the particles carried by the flue gas from coal-fired power plants. Within a certain volume, the particles were smaller and the number of particles was more. These small particles are more capable of migration and have a significant health and environmental impact. Therefore, attention must be paid to the particles carried by the ascending geogas flow from concealed deposits.

Such sulfur-containing particles enter the atmosphere. Several studies have discussed the direct effects of sulfate particles on the climate (Liu et al., 2009). Some researchers have suggested that sulfur-containing particles can reduce atmospheric temperature or result in climate warming. Streets et al. (2000) suggested that because sulfate aerosols play a vital role in cooling the atmosphere, a reduction in sulfur dioxide emissions in the future would result in increased global warming. Furthermore, aerosol sulfate has been identified as an important contributor to sunlight scattering (Lelieveld and Heintzenberg, 1992; Kim et al., 2001). At the top of the atmosphere above East Asia, $SO_4^{2-}$ radiative forcing is −2 to −10 W $m^{-2}$ over land and −5 to −15 W $m^{-2}$ over ocean (Gao et al., 2014). Niemeier et al. (2011) revealed that an increase in the $SO_2$ emission rate does not lead to a similar increase in radiative forcing because, as the size of the aerosols increases, their lifetime decreases. It is thus possible that the sulfur-containing particles transported by an ascending geogas flow have an effect on the climate and should, therefore, be evaluated.

Sulfate particles can be transported into the lungs leading to respiratory illnesses (World Bank Group, 1999; Soleimani et al., 2007). In particular, the sulfur-containing particles contain high levels of toxic Pb, Hg, Cu, and As. In nature, sulfur usually combines with Pb, Hg, Cu, As, Ni, Cd, and Sb, which are toxic to organisms, to form sulfide deposits. The sulfur-containing particles originating from sulfide deposits commonly contain toxic elements. This phenomenon has been confirmed by EDX analysis of particles. The particle sizes carried by the ascending gas flow are usually less than 500 nm. The size is only one-fifth of the upper size limit of PM2.5. Geogas particles undergo long-distance migration. They can remain in the atmosphere for long periods and in can get into bronchioles and alveoli, affecting the ventilative function of lung. They can also enter the blood. The possible relationship between the occurrence of sulfur-containing particles transported by an ascending geogas flow and endemic diseases in the vicinity of sulfur-containing deposits should be investigated.

It is probable that sulfur-containing particles transported by the ascending geogas flows in the soil affect the soil system; for example, sulfur-containing particles can affect both soil biota and enzymatic activities, resulting in changes in the soil structure, nutrient cycling, and organic matter decomposition and retention. Sulfur-containing particles may directly catalyze organic matter decomposition. Furthermore, the potential use of such particles as fertilizers for rice plants needs to be investigated.

Acknowledgments

Financial support from the National Natural Science Foundation of China (Grant Nos. 41030425, 41072263, 40773037, and 40673044) and the National High-Tech

297 Research and Development Program of China (863 Program; Grant No.
298 2008AA06Z101) are gratefully acknowledged.

299 References

300 Andres, R. J., Rose, W. I., Stoiber, R. E., Williams, S. N., Matías, O., and Morales, R.:
301 A summary of sulfur dioxide emission rate measurements from Guatemalan
302 volcanoes, B. Volcanol., 55, 379–388, 1993.

303 Bao, H. M., Yu, S., and Tong, D. Q.: Massive volcanic $SO_2$ oxidation and sulphate
304 aerosol deposition in Cenozoic North America, Nature, 465, 909–912, 2010.

305 Berresheim H.: Biogenic sulfur emissions from the Subantarctic and Antarctic Oceans,
306 J. Geophys. Res.. 92, 13245–13262, 1987.

307 Bhugwant, C., Siéja, B., Bessafi, M., Staudacher, T., and Ecormier, J.: Atmospheric
308 sulfur dioxide measurements during the 2005 and 2007 eruptions of the Piton de
309 La Fournaise volcano: Implications for human health and environmental changes,
310 J. Volcanol. Geoth. Res., 184, 208–224, 2009.

311 Cao, J. J.: Migration mechanisms of gold nanoparticles explored in geogas of the
312 Hetai ore district, southern China, Geochem. J., 45, e9–e13, 2011.

313 Cao, J. J., Hu, R. Z., Liang, Z. R., and Peng, Z. L.: TEM observation of
314 geogas-carried particles from the Changkeng concealed gold deposit, Guangdong
315 Province, South China, J. Geochem. Explor. 101, 247–253, 2009.

316 Cao, J. J., Hu, X. Y., Jiang, Z. T., Li, H. W., and Zou, X. Z.: Simulation of adsorption
317 of gold nanoparticles carried by gas ascending from the Earth's interior in
318 alluvial cover of the middle-lower reaches of the Yangtze River, Geofluids, 10,

438–446, 2010a.

Cao, J. J., Liu, C., Xiong, Z. H., and Qin, T. R.: 2010b, Particles carried by ascending gas flow at the Tongchanghe copper mine, Guizhou Province, China, Science China Earth Sciences, 53, 1647–1654, 2010b.

Cao, J. J., Liu, C., Zhang, P,, Li, Y. P., and Xiong, Z. H.: The characteristic of geogas particles from Daheishan basalt copper deposit in the Huize county of Yunnan, Mital Mine, 113–115, 2011 (in Chinese with English abstract).

Chenet, A. L., Fluteau, F., and Courtillot, V.: Modelling massive sulfate aerosol pollution, following the large 1783 Laki basaltic eruption, Earth Planet. Sc. Lett., 236, 721–731, 2005.

Etiope, G., and Martinelli, G., Migration of carrier and trace gases in the geosphere: an overview, Phys. Earth Planet. In., 129, 185–204, 2002.

Gao Y., Zhao C., Liu X. H., Zhang, M. G., and Leung, L. R.: WRF-Chem simulations of aerosols and anthropogenic aerosol radiative forcing in East Asia. Atmos. Environ., 92, 250–266, 2014.

Gierć, R., and Querol, X.: 2010, Atmospheric particles: solid particulate matter in the atmosphere. Elements, 6, 215–222, 2010.

Graf, H.-F., Langmann, B., and Feichter, J.: The contribution of Earth degassing to the atmospheric sulfur budget, Chem. Geol.. 147, 131–145, 1998.

Holub, R. F., Hovorka, J., Reimer, G. M., Honeyman, B. D., Hopke, P. K., and Smrz P. K.: Further investigations of the "geoaerosol" phenomenon, J. Aerosol Sci., 32, 61–70, 2001.

341 Holub, R. F., Reimer, G. M., Hopke, P. K., Hovorka, J., Krcmar, B., and Smrz, P. K.:
342 "Geoaerosols": their origin, transport and paradoxical behavior: a challenge to
343 aerosol science, J. Aerosol Sci., 30, S111–S112, 1999.
344 Kim, B. G., Park, S. U., and Han, J. S: Transport of $SO_2$ and aerosol over the Yellow
345 sea, Atmos. Environ., 35, 727–737, 2001.
346 Kristmannsdottir, H., Sigurgeirsson, M., Armannsson, H., Hjartarson, H., and
347 Olafsson, M., Sulfur gas emissions from geothermal power plants in Iceland,
348 Geothermics, 29, 525–538, 2000.
349 Lelieveld, J., and Heintzenberg, J.: Sulfate cooling effect on climate through in-cloud
350 oxidation of anthropogenic $SO_2$, Science, 258, 117–120, 1992.
351 Liu, C., Cao, J. J., and Ke, H. L.: Geogas characteristic of Yongshengde copper ores in
352 the Northeastern Yunnan, China, Geology of Chemical Minerals, 33, 201–207,
353 2011(in Chinese with English abstract).
354 Liu, Y., Sun, J. R., and Yang, B.: The effects of black carbon and sulfate aerosols in
355 China regions on East Asia monsoons, Tellus B, 61, 642–656, 2009.
356 Niemeier, U., Schmidt, H., and Timmreck, C.: The dependency of geoengineered
357 sulfate aerosol on the emission strategy, Atmos. Sci. Lett. Special Issue:
358 Geoengineering, 12, 189–194, 2011.
359 Pósfai, M., Anderson, J. R., and Buseck, P. R.: Soot and sulfate aerosol particles in the
360 remote marine atmosphere, in: Geological Society of America, 1997 annual
361 meeting, Abstracts with Programs - Geological Society of America, 29, 357,
362 1997.

Qi, L. Q., Yuan, Y.T., and Liu, J.: Current situations of emission and collection on fly ash of power plants in China: International Conference on Power Engineering-2007, Hangzhou, China, 23 – 27 October 2007, 766 – 772, 2007.

Rose, W. I., Chuan, R. L., Giggenbach, W. F., Kyle, P. R., and Symonds, R. B.: Rates of sulfur dioxide and particle emissions from White Island volcano, New Zealand, and an estimate of the total flux of major gaseous species, B. Volcanol., 48, 181–188, 1986.

Seino, N., Sasaki, H., Sato, J., and Chiba, M.: High-resolution simulation of volcanic sulfur dioxide dispersion over the Miyake Island, Atmos. Environ., 38, 7073–7081, 2004.

Sinninghe Damsté, J. S., Irene, W., Rijpstra, C., de Leeuw, J. W., and Schenck, P. A.: 1988, Origin of organic sulfur compounds and sulfur-containing high molecular weight substances in sediments and immature crude oils, Org. Geochem., 13, 593–606, 1988.

Soleimani, M., Bassi, A., and Margaritis A.: Biodesulfurization of refractory organic sulfur compounds in fossil fuels, Biotechnol. Adv., 25, 570–596, 2007.

Streets, D. G., Tsai, N. Y., Akimoto, H., and Oka, K.: Sulfur dioxide emissions in Asia in the period 1985–1997, Atmos. Environ., 34, 4413–4424, 2000.

Sweeney, D., Kyle, P. R., and Oppenheimer, C.: Sulfur dioxide emissions and degassing behavior of Erebus volcano, Antarctica, J. Volcanol. Geoth. Res., 177, 725–733, 2008.

Tong, C. H., and Li, J. C.: A new method searching for concealed mineral resources:

385 geogas prospecting based on nuclear analysis and accumulation sampling, J.
386 China Univ. Geosci., 10, 329–332, 1999.
387 Trabue, S., Scoggin, K., Mitloehner, F., Li, H., Burns, R., and Xin, H. W.: Field
388 sampling method for quantifying volatile sulfur compounds from animal feeding
389 operations, Atmos. Environ., 42, 3332–3341, 2008.
390 Wei, X. J., Cao, J. J., Holub, R. F., Hopke, P. K., and Zhao, S, J.: TEM study of
391 geogas-transported nanoparticles from the Fankou Lead-Zinc Deposit,
392 Guangdong Province, South China, J. Geochem. Explor., 128, 124–135, 2013.
393 Williams, K. D., Jones, A., Roberts, D. L., Senior, C. A., and Woodage, M. J.: The
394 response of the climate system to the indirect effects of anthropogenic sulfate
395 aerosol, Clim. Dynam., 17, 845–856, 2001.
396 Wong, M. H.: An ecological survey of the effect of sulfur dioxide emitted from an
397 Acid Work Factory, B. Environ. Contam. Tox., 19, 715–723, 1978.
398 World Bank Group: Pollution prevention and abatement handbook: towards cleaner
399 production, World Bank Group Publishers, Washington DC, 1999, 1998.
400 Wu, T., Wang, X. M., Li, D. J., and Yi, Z. G.: Emission of volatile organic sulfur
401 compounds (VOSCs) during aerobic decomposition of food wastes, Atmos.
402 Environ., 44, 5065–5071, 2010.
403 Yang, F. G., and Tong, C. H.: Geogas anomaly and mechanism in Xuanhan gas field,
404 Earth Science-Journal of China University of Geosciences, 2000, 25, 103–106
405 (in Chinese with English abstract).
406 Yang, Z., Kanda, K., Tsuruta, H., and Minami, K.: Measurement of biogenic sulfur

gases emission from some Chinese and Japanese soils, Atmos. Environ., 30, 2399–2405, 1996.

Yang, Z., Kong, U. L., Zhang, J., Wang, L., and Xia, S.: Emission of biogenic sulfur gases from Chinese rice paddies, Sci. Total Environ., 224, 1–8, 1998.

Zhang, C. F, Yao, Q., and Sun, J. M.: Characteristics of particulate matter from emissions of four typical coal-fired power plants in China, Fuel Process Technol., 86, 757– 768, 2005.

Zreda-Gostynska, G., Kyle, P., and Finnegan, D.: Chlorine, fluorine, and sulfur emissions from Mount Erebus, Antarctica and estimated contributions to the Antarctic atmosphere, Geophys. Res. Lett., 20, 1959–1962, 1993.

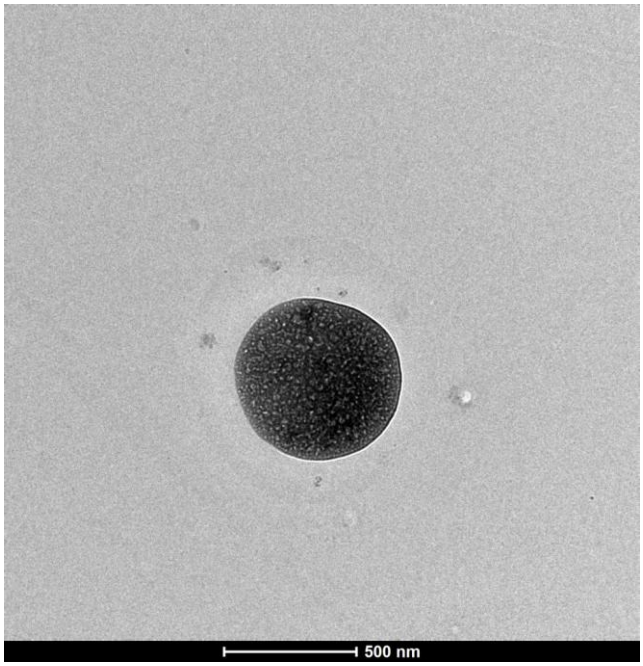


Fig. 1 TEM image of an S-, O-, and Si-containing particle obtained from an ascending gas flow above the soil over the Dongshengmiao deposit.

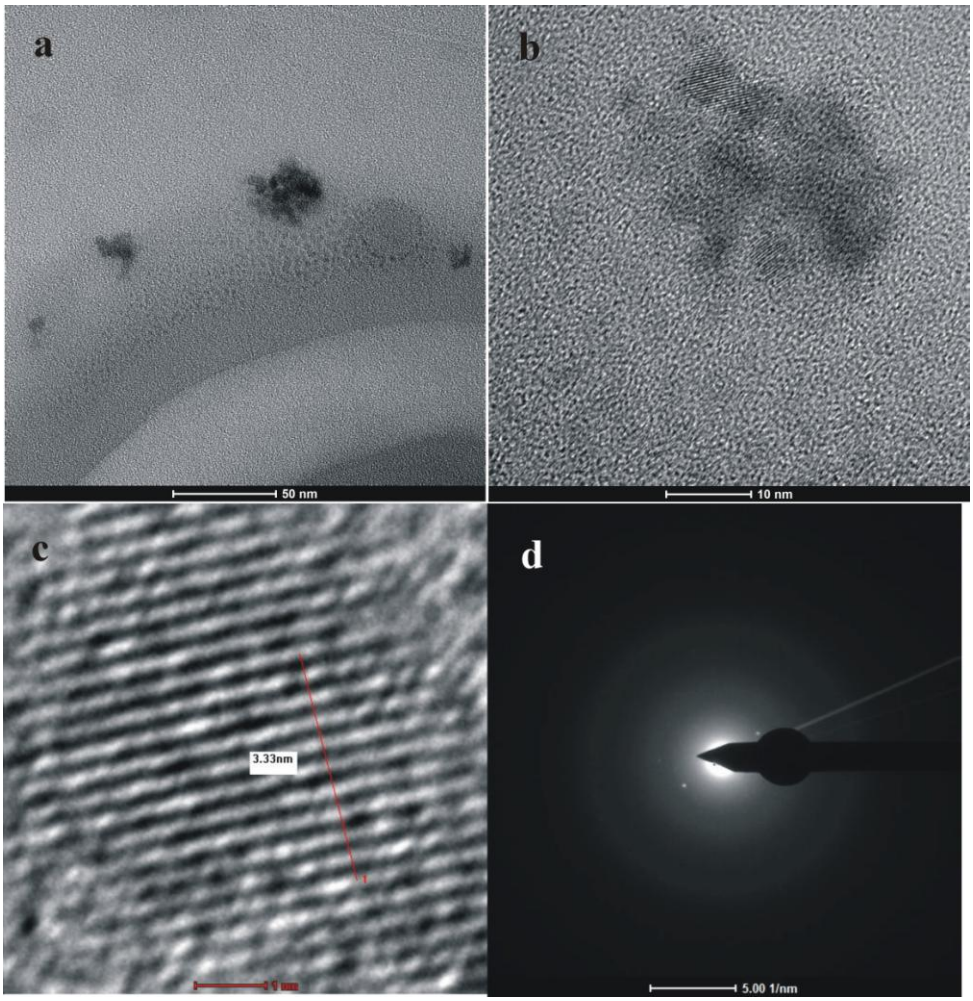


Fig. 2 (a) TEM image, (b, c) high-resolution (HRTEM) images, and (d) selected area electron diffraction (SAED) pattern of an S-, O-, Hg-containing particle aggregation obtained from an ascending gas flow above the soil over the Dongshengmiao deposit.

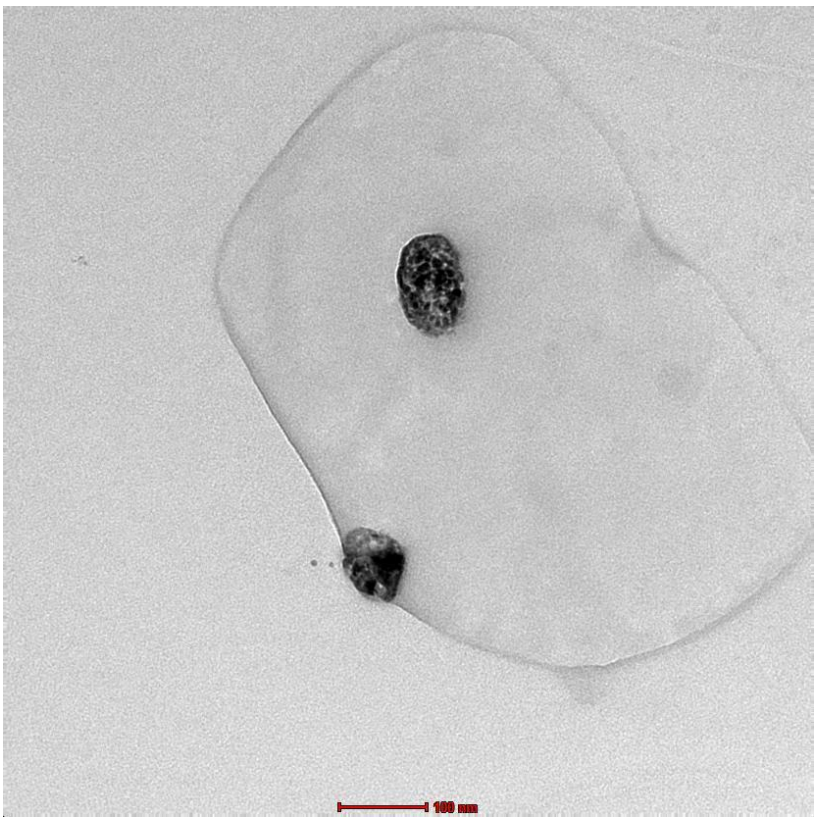


Fig. 3 TEM image of S-, O-, K-, and Pb-containing particle aggregations obtained from an ascending gas flow above the soil over the Dongshengmiao deposit.

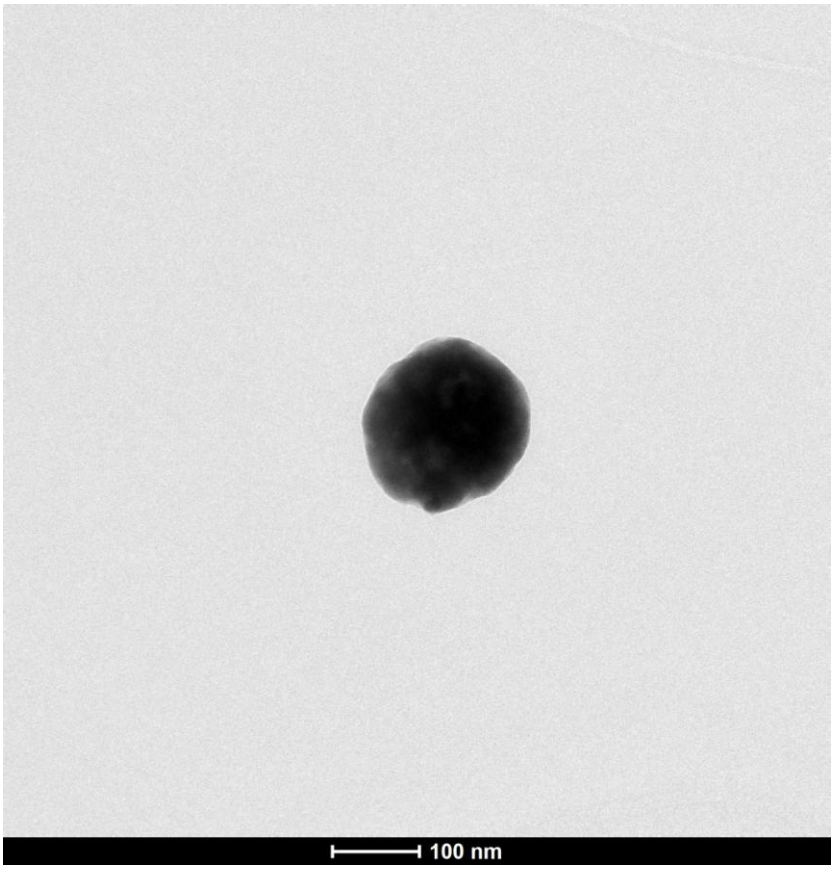


Fig. 4 TEM image of an S-, O-, Na-, Pb-, Zn-, and As-containing particle obtained from an ascending gas flow above the soil over the Dongshengmiao deposit.

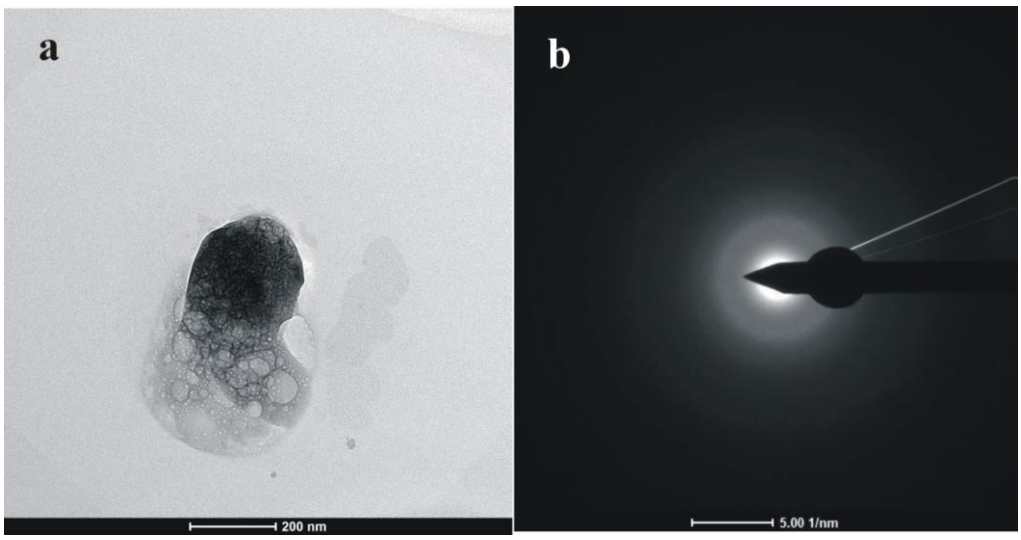


466 Fig. 5 (a) TEM image and (b) SAED pattern of an S-, O-, K-, Na-, and Pb-containing
467 particle obtained from an ascending gas flow above the soil over the Dongshengmiao
468 deposit.

469

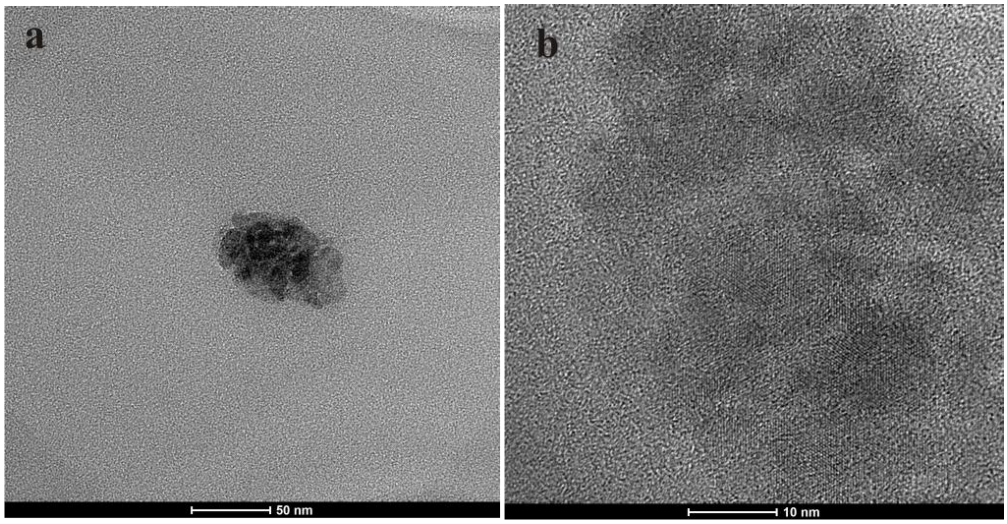


470 Fig. 6 (a) TEM image and (b) HRTEM image of an O-, Si-, S-, and Cu-containing
471 particle aggregation obtained from an ascending gas flow above the soil over the
472 Dongshengmiao deposit.

473

474

475

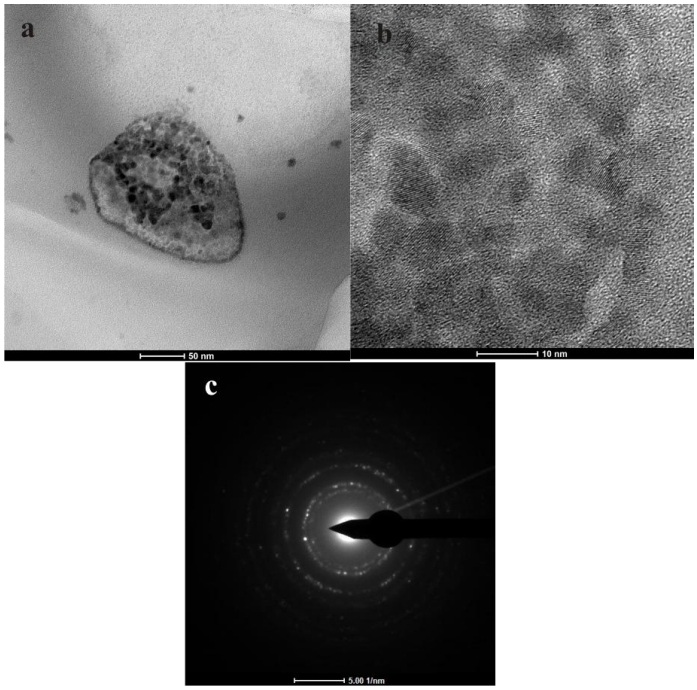


Fig. 7 (a) TEM image, (b)HRTEM image, and (c) SAED pattern of an O-, S-, K-, and Pb-containing particle aggregation obtained from an ascending gas flow above the soil over the Dongshengmiao deposit.

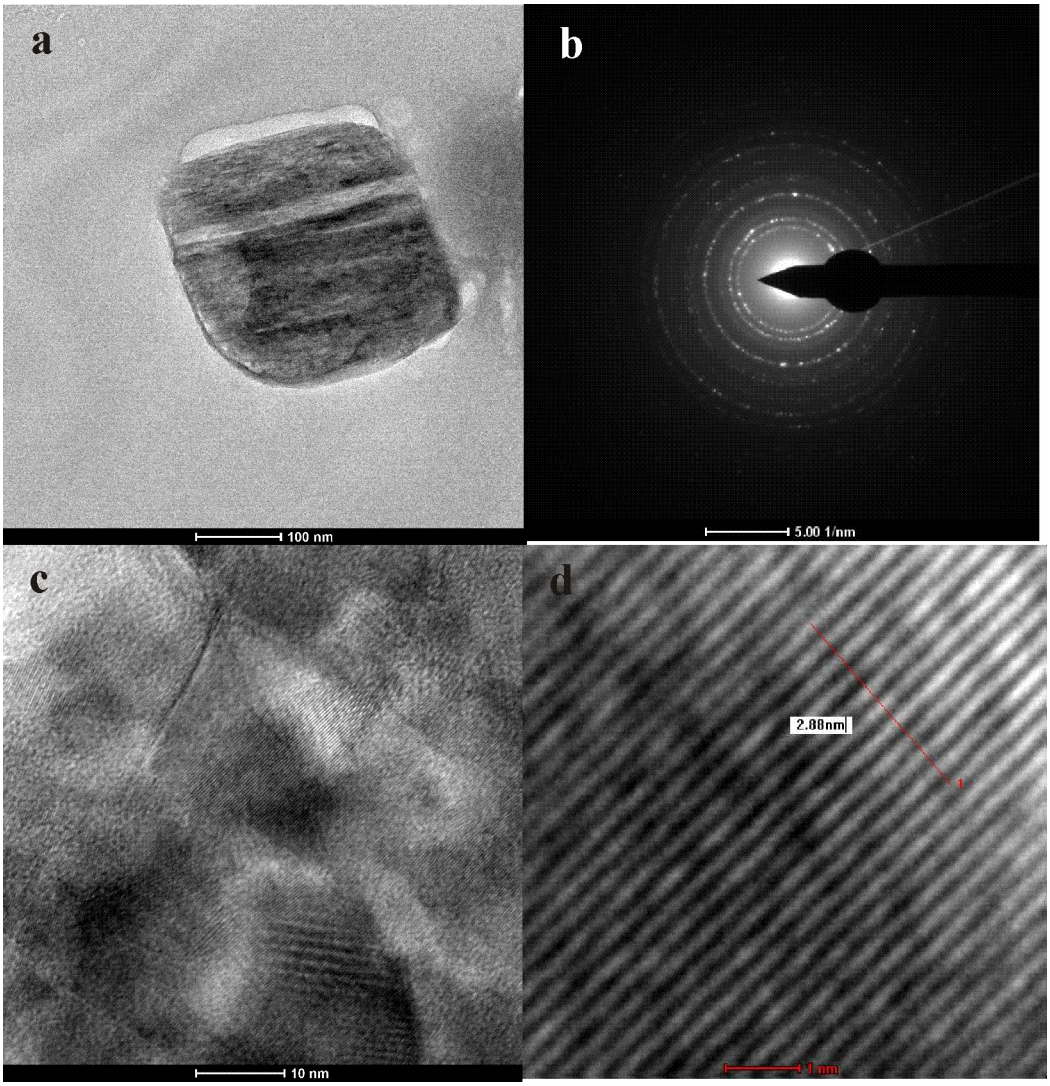


Fig. 8 (a) TEM image, (b) SAED pattern, and (c, d) HRTEM image of an O-, S-, Ca-, and Mg-containing particle obtained from an ascending gas flow in the soil over Dongshengmiao deposit.

510

511

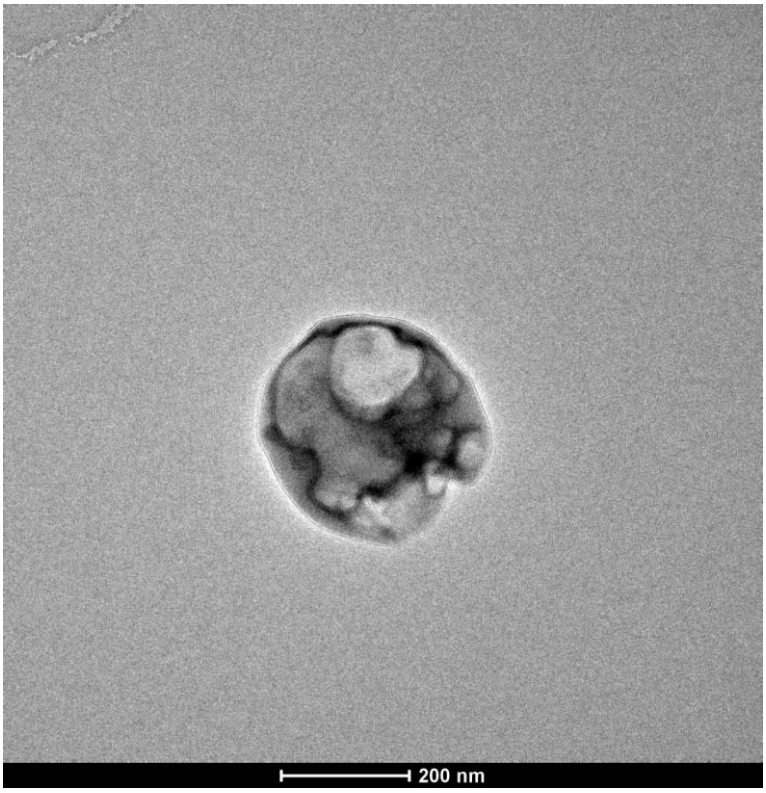


512

513 Fig. 9 TEM image of an O-, S-, and K-containing particle obtained from an ascending

514 gas flow in the soil from the Kafang copper deposit, Yunnan Province.

515

516

517

518

519

520

521

522

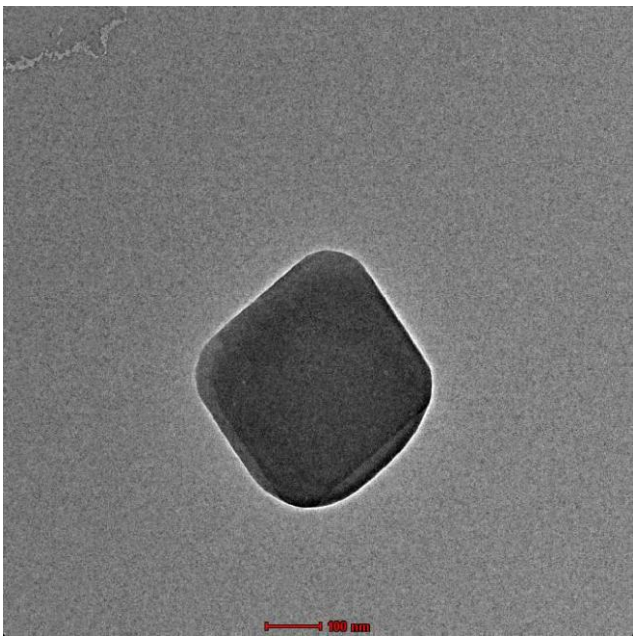

Fig. 10 TEM image of an O-, S-, and Fe-containing particle obtained from an ascending gas flow in the soil from the Yongshengde copper deposit in northeastern Yunnan.

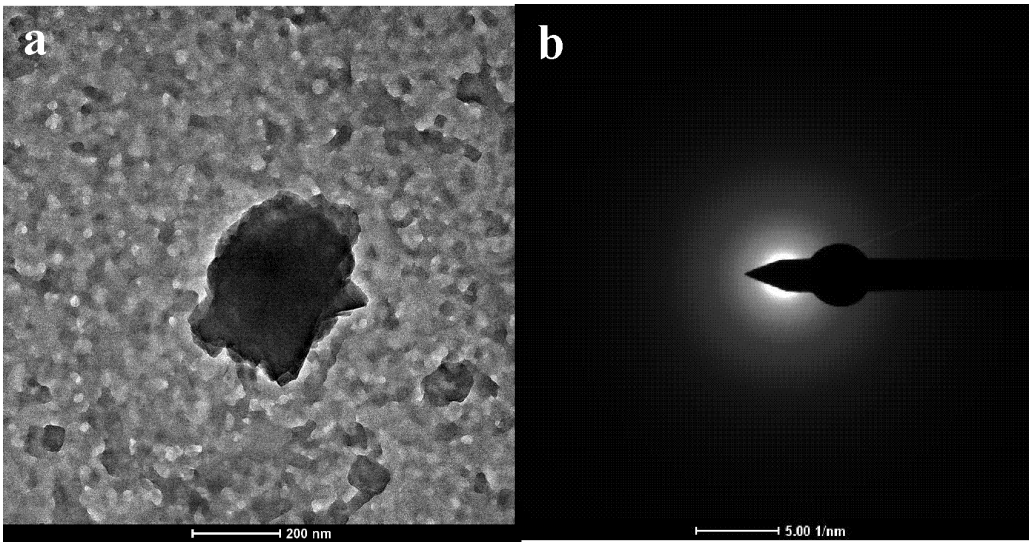


Fig. 11 (a) TEM image and (b) SAED pattern of an O-, S-, and Co-containing particle obtained from an ascending gas flow in the soil from the Qingmingshan Cu–Ni sulfide deposit, Guangxi Province.

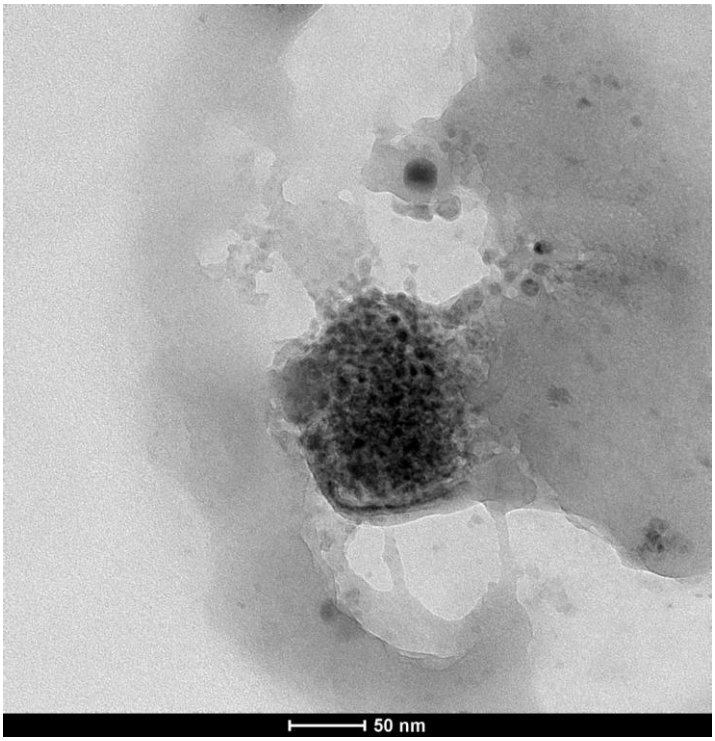


Fig. 12 TEM image of an O-, S-, K-, Pb-, and Na-containing particle sampled using a vacuum pump from the fault gas near a concealed ore body of the Dongshengmiao deposit.

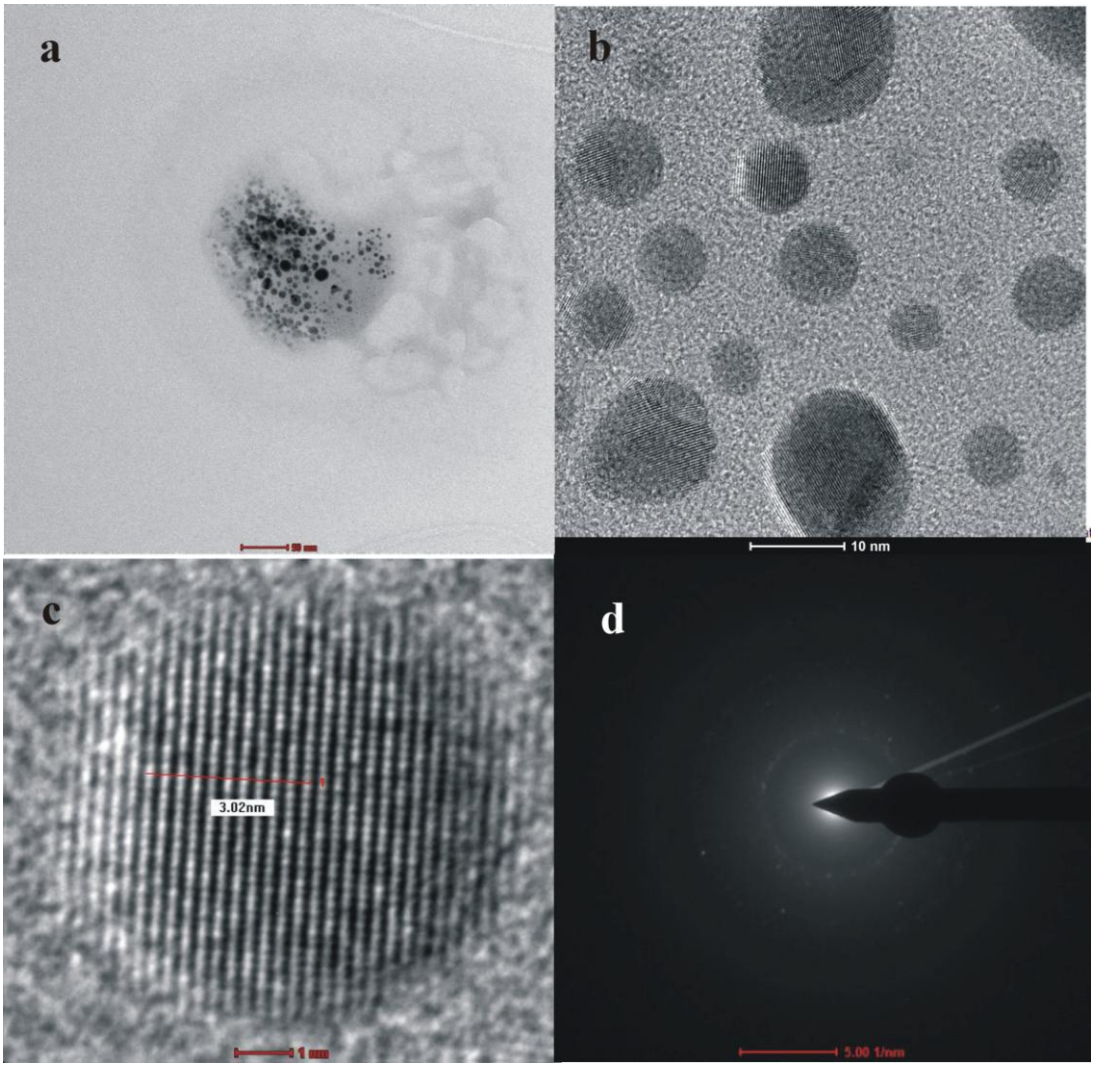


Fig. 13 (a) TEM image, (b, c) HRTEM images, and (d) SAED pattern of an O-, S-, and K-containing particle aggregation sampled using a PVC pipe in a fault near a concealed ore body of the Dongshengmiao deposit.

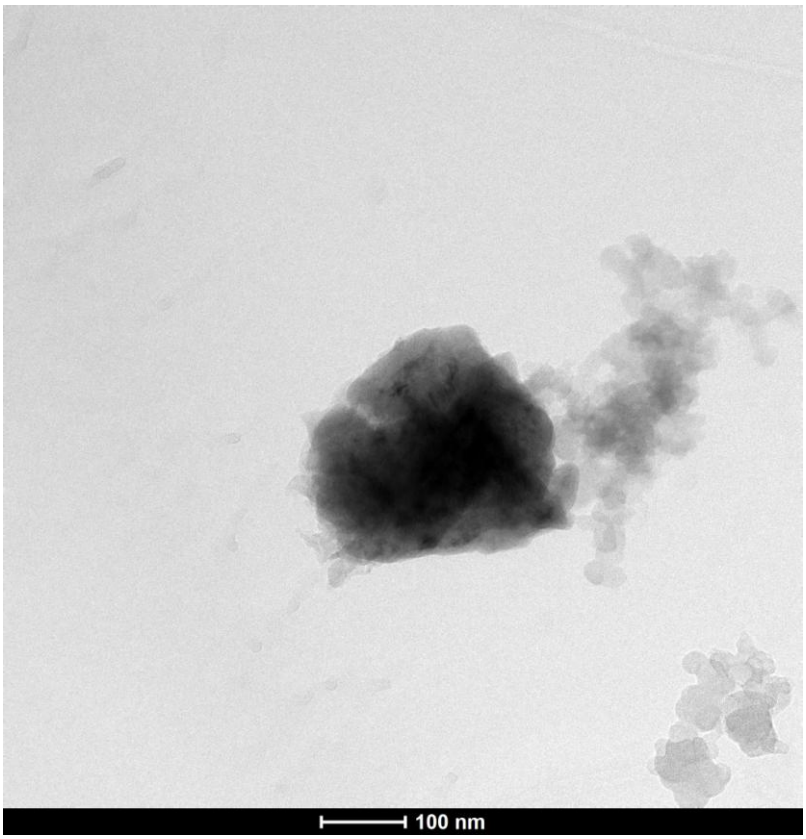


Fig. 14 TEM image of an O-, S-, Fe-, and Mg-containing particle aggregation sampled using a PVC pipe in a fault above a concealed ore body of the Dongshengmiao deposit.

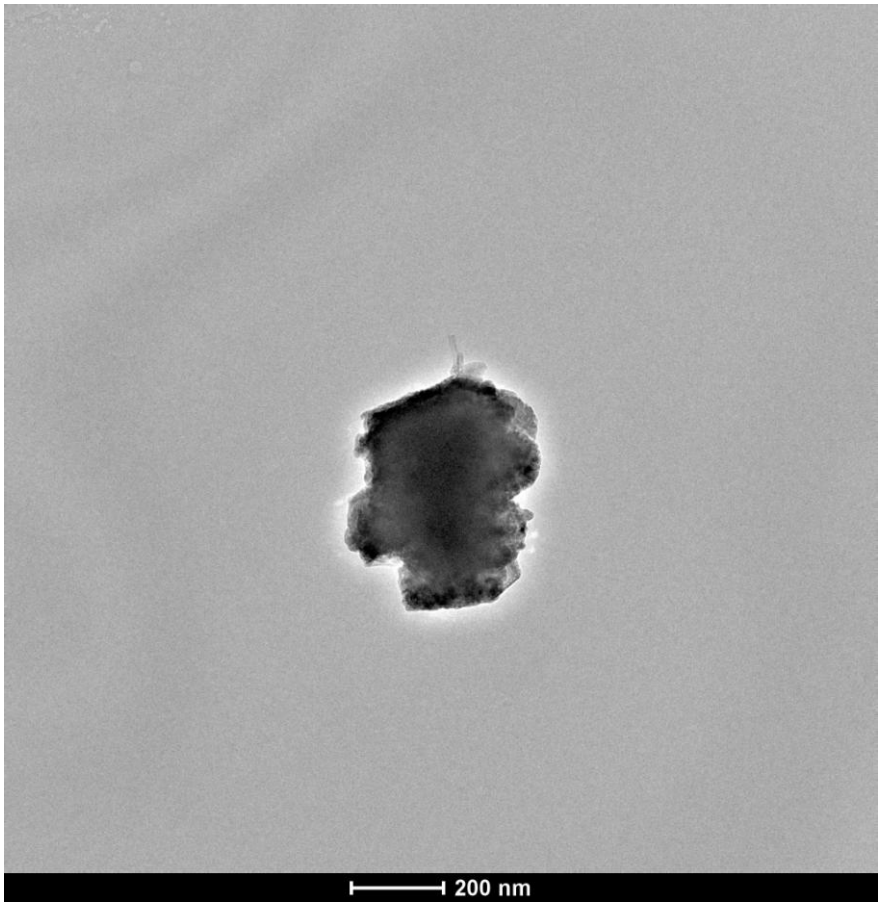


Fig. 15 TEM image of an O-, S-, Ti-, Sr-, and Ba-containing particle from a deep-seated oxidized zone in the Dongshengmiao deposit.

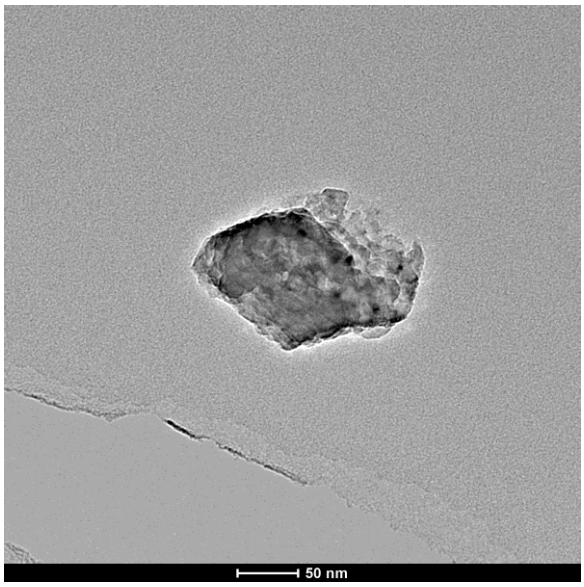


Fig. 16 TEM image of an O-, S-, Fe-, Co-, and Ca-containing particle from a deep-seated fault gouge in the Dongshengmiao deposit.

Table 1 Number of sulfur-containing particles or particle aggregations number from the Dongshengmiao deposit on 100 μm × 100 μm TEM grids

| Sulfur-containing particles or particle aggregations carried by ascending gas flow above the soil (that had flown through the soil) | | | | Sulfur-containing particles or particle aggregations carried by ascending gas flow in deep faults | | | |
|---|---|---|---|---|---|---|---|
| Sample | Sample box | Grid | Number | Sample | Sample box | Grid | Number |
| ND13-1 | A1 | A1-1 | 3 | NDDW03 | A2 | A2-2 | 3 |
| ND13-2 | A2 | A2-1 | 2 | NDDW05 | A4 | A4-1 | 1 |
| ND13-3 | A3 | A3-2 | 1 | | | A4-2 | 29 |
| | | A3-3 | 6 | NDDW06 | A5 | A5-2 | 1 |
| ND13-4 | A4 | A4-1 | 1 | NDDW07 | B1 | B1-1 | 4 |
| | | A4-2 | 2 | | | B1-2 | 1 |
| ND13-6 | A5 | A5-1 | 1 | NDDW19 | D3 | D3-2 | 1 |
| | | A5-2 | 3 | | | D3-3 | 2 |
| | | A5-3 | 1 | NDDW26 | E4 | E4-1 | 1 |
| ND13-8 | B2 | B2-1 | 1 | | | E4-3 | 1 |
| | | B2-2 | 6 | NDDW27 | E5 | E5-1 | 2 |
| | | B2-3 | 1 | | | E5-3 | 2 |
| ND13-9 | B3 | B3-1 | 1 | | | E5-4 | 1 |
| | | B3-2 | 1 | NDDW36 | G4 | G4-1 | 12 |
| | | B3-3 | 1 | | | G4-3 | 10 |
| ND13-10 | B4 | B4-1 | 1 | | | G4-4 | 1 |
| | | B4-3 | 6 | NDDW37 | G5 | G5-1 | 1 |
| ND13-11 | B5 | B5-1 | 1 | | | | |

Table 2 EDX results for particles 1–8.

| Element | Particle number | | | | | | | |
|---|---|---|---|---|---|---|---|---|
| | 1 | 2 | 3 | 4 | 5 | 6 | 7 | 8 |
| Weight O% | 18.47 | 9.46 | 16.02 | 9.73 | 15.75 | 12.9 | 5.13 | 51.88 |
| Atomic O% | 31.1 | 31.78 | 31.12 | 39.3 | 34.16 | 31.35 | 22.74 | 69.78 |
| Weight Si% | 3.35 | | 1.49 | 0.5 | 1.09 | 3.08 | | 2.19 |
| Atomic Si% | 3.21 | | 1.65 | 1.15 | 1.34 | 4.27 | | 1.67 |
| Weight S% | 78.17 | 31.23 | 63.1 | 3.82 | 10.83 | 21.61 | 18.25 | 19.02 |
| Atomic S% | 65.68 | 52.33 | 61.16 | 7.7 | 11.72 | 26.2 | 40.32 | 12.76 |
| Weight Hg% | | 59.29 | | | | | | |
| Atomic Hg% | | 15.87 | | | | | | |
| Weight K% | | | 4.88 | | 35.75 | | 7.31 | 0.99 |
| Atomic K% | | | 3.88 | | 31.73 | | 13.25 | 0.54 |
| Weight Pb% | | | 14.48 | 54.2 | 22.5 | | 69.28 | |
| Atomic Pb% | | | 2.17 | 16.9 | 3.76 | | 23.67 | |
| Weight Na% | | | | 3.1 | 9.66 | | | |
| Atomic Na% | | | | 8.73 | 14.58 | | | |
| Weight Fe% | | | | 0.75 | 2.14 | | | 0.21 |
| Atomic Fe% | | | | 0.87 | 1.33 | | | 0.08 |
| Weight Co% | | | | 0.98 | 2.25 | | | |
| Atomic Co% | | | | 1.08 | 1.32 | | | |
| Weight Zn% | | | | 8.34 | | | | |
| Atomic Zn% | | | | 8.24 | | | | |
| Weight As% | | | | 18.55 | | | | |
| Atomic As% | | | | 16 | | | | |
| Weight Cu% | | | | | | 62.39 | | |
| Atomic Cu% | | | | | | 38.16 | | |
| Weight Mg% | | | | | | | | 3.86 |
| AtomicMg% | | | | | | | | 3.42 |
| Weight Ca% | | | | | | | | 21.82 |
| Atomic Ca% | | | | | | | | 11.71 |

Table 3 EDX results for particles 9–16.

| Element | Particle number | | | | | | | |
|---|---|---|---|---|---|---|---|---|
| | 9 | 10 | 11 | 12 | 13 | 14 | 15 | 16 |
| Weight O% | 26.54 | 56.25 | 53.66 | 25.39 | 67.03 | 17.21 | 29.21 | 40.8 |
| Atomic O% | 42.51 | 73.54 | 70.2 | 37.32 | 80.72 | 35.83 | 64.85 | 62.97 |
| Weight Si% | 0.52 | | | 0.66 | 1 | 0.7 | | 1.5 |
| Atomic Si% | 0.47 | | | 0.55 | 0.68 | 0.83 | | 1.32 |
| Weight S% | 63.99 | 31.3 | 42.81 | 23.8 | 28.01 | 24.59 | 10.88 | 15.03 |
| Atomic S% | 51.15 | 20.42 | 27.95 | 17.45 | 16.83 | 25.53 | 12.05 | 11.58 |
| Weight K% | 8.93 | 0.78 | | 2.01 | 2.59 | | | |
| Atomic K% | 5.85 | 0.42 | | 1.21 | 1.27 | | | |
| Weight Pb% | | | | 4.25 | | | | |
| Atomic Pb% | | | | 0.48 | | | | |
| Weight Na% | | | 1.04 | 40.92 | | 1.35 | | |
| Atomic Na% | | | 0.95 | 41.84 | | 1.96 | | |
| Weight Fe% | | 9.94 | 0.44 | 1.11 | 1.35 | 51.16 | 1.27 | 5.2 |
| Atomic Fe% | | 3.72 | 0.16 | 0.46 | 0.46 | 30.5 | 0.81 | 2.3 |
| Weight Co% | | | 2.03 | | | | | 6.36 |
| Atomic Co% | | | 0.72 | | | | | 2.66 |
| Weight Zn% | | | | 1.82 | | | | |
| Atomic Zn% | | | | 0.65 | | | | |
| Weight Mg% | | | | | | 2.74 | | |
| Atomic Mg% | | | | | | 3.75 | | |
| Weight Ca% | | | | | | 0.28 | 0.5 | 31.08 |
| Atomic Ca% | | | | | | 0.23 | 0.44 | 19.15 |
| Weight F% | | 1.71 | | | | | | |
| Atomic F% | | 1.88 | | | | | | |
| Weight Al% | | | | | | 0.25 | | |
| Atomic Al% | | | | | | 0.3 | | |
| Weight Mn% | | | | | | 1.68 | | |
| Atomic Mn% | | | | | | 1.02 | | |
| Weight Ti% | | | | | | | 10.94 | |
| Atomic Ti% | | | | | | | 8.11 | |
| Weight Sr% | | | | | | | 10.32 | |
| Atomic Sr% | | | | | | | 4.18 | |
| Weight Ba% | | | | | | | 36.86 | |
| Atomic Ba% | | | | | | | 9.53 | |